TABLE I
FIRST STEPS OF THE ITERATION.

$\|z\|$	N_1	N_2	N_3	N
$1.105 \cdot 10^{-60}$	1.94	2.00	2.00	2
$5.025 \cdot 10^{-15}$	7.42	7.97	8.00	8
0.0039382	27.92	31.88	32.00	32
4.52642	99.99	100.00	100.00	100
63.2614	270.76	257.98	256.27	256
146.318	399.93	399.99	400.00	400
1314.061	1998.82	2048.82	2047.99	2048
11849.408	16318.90	16384.25	16384.00	16384

than a certain upper limit, has been presented. This is a useful procedure for avoiding numerical overflow when $|z|$ is very small compared to the orders involved in the calculation.

ACKNOWLEDGMENT

The computation of Bessel functions was studied by the author as part of his Ph.D. research under supervision of Prof. J. H. Cloete at the University of Stellenbosch.

REFERENCES

[1] R. F. Harrington, *Time-Harmonic Electromagnetic Fields*. New York: McGraw-Hill, 1961.
[2] M. Goldstein and R. M. Thaler, "Recurrence techniques for the calculation of Bessel functions," in *Math. Tables and Other Aids to Comput.*, vol. 13, pp. 102–108, 1959.
[3] I. A. Stegun and M. Abramowitz, "Generation of Bessel functions on high speed computers," in *Math. Tables and other Aids to Comput.*, vol. 11, pp. 255–257, 1957.
[4] Y. L. Luke, "Miniaturized tables of Bessel functions III," *Math. Comp.*, vol. 26, pp. 237–240, Jan. 1972.
[5] E. Amos, "A portable package for Bessel functions of a complex argument and nonnegative order," *ACM Trans. Mathematical Software*, vol. 12, pp. 265–273, Sept. 1986.
[6] J. B. Campbell, "Bessel functions $J_\nu(x)$ and $Y_\nu(x)$ of real order and real argument," *Comput. Phys. Commun.*, vol. 18, pp. 133–142, 1979.
[7] C. F. du Toit, "The numerical computation of Bessel functions of the first and second kind for integer orders and complex arguments," *IEEE Trans. Antennas Propagation*, vol. 38, pp. 1341–1349, Sept. 1990.
[8] C. F. du Toit, "Evaluation of some algorithms and programs for the computation of integer-order Bessel functions of the first and second kind with complex arguments," *IEEE Antennas Propagation*, vol. 35, pp. 19–25, June 1993.
[9] F. W. J. Olver, "Bessel functions of integer order," in *Handbook of Mathematical Functions*, M. Abramowitz and I. A. Stegun, eds., ch. 9. Washington, DC: National Bureau of Standards, 1964.

An SEM Analysis of the Voltage Induced upon a Printed Strip Antenna by a Transient Plane Wave

George W. Hanson

***Abstract*—The singularity expansion method (SEM) is applied to study the interaction of a transient electromagnetic plane wave with a printed strip antenna. The SEM is an attractive technique for this problem since the time-domain response of the element is separated into excitation-independent natural resonances and modes, which have considerable physical significance, and closed-form coupling terms which can be rapidly evaluated as the geometric or temporal properties of the source change. The purpose of this work is to demonstrate the SEM as applied to the transient microstrip problem, and to study the effect of varying the properties of the printed circuit substrate over a range of values typically found in microstrip antenna applications. The transient response due to a step and Gaussian excitation is studied, where it is found that the level of transient signal induced on a printed element increases with increasing substrate thickness and decreases with increasing substrate permittivity. The shape of the induced voltage or current waveform is highly dependent on the geometric and temporal properties of the source for elements printed on relatively thin substrates, while the elements printed on thicker substrates the shape of the induced waveform is much less sensitive to the form of the excitation, and resembles the oscillation of the fundamental resonance of the antenna.**

Manuscript received May 3, 1993; revised July 26, 1993.

The author is with the Department of Electrical Engineering and Computer Science, University of Wisconsin-Milwaukee, Milwaukee, WI 53201.

IEEE Log Number 9214102.

I. INTRODUCTION

With the increasing use of microstrip antennas and circuits, the transient behavior of printed conductors in the layered microstrip geometry is receiving attention. Analytical expressions for the transient radiation field of a Hertzian microstrip dipole embedded in a lossless grounded dielectric slab, with both vertical and horizontal polarizations, has been developed [1]. Also in [1], analytical expressions for the transient radiation field of a microstrip transmission line with a known current distribution are obtained. The transient voltages and currents induced on a microstrip line by an electromagnetic (EM) field has been studied using a distributed-source transmission-line model [2]. The interaction of a transient EM pulse with a microstrip patch antenna has been analyzed using a finite difference scheme [3], also with the identification of an analytical equivalent circuit.

The purpose of this work is to analyze the behavior of a microstrip dipole element excited by a transient plane wave. Microstrip antennas are used in air and spacecraft applications since they are lightweight and conformal. These antennas may be exposed to external transient fields of man-made origin, such as short-pulse radar, or natural sources such as lightning. In almost all cases the incident field can be modeled by a plane wave with a prescribed temporal behavior.

The singularity expansion method (SEM) [4], [5] is used here, which yields accurate results in closed form subsequent to identification of the element's natural resonances and natural modes, and provides good physical insight into the interaction of a transient EM field with a microstrip element. A previous paper [6] presented results from application of the SEM to the time-harmonic radar cross section (RCS) analysis of a microstrip dipole. That work is extended here to include the transient microstrip problem. It is found that the late-time transient SEM current can be represented as a simple residue series, similar to the free-space object case, even though the microstrip element resides in a layered media background. This background environment supports surface waves and introduces dielectric loss to the system, and is accounted for by using an appropriate microstrip Green's function.

II. THEORY

The printed strip geometry with a lumped load impedance Z_L is shown in Fig. 1. An α-polarized transient EM plane wave, $\vec{E}^i(\vec{r}, t) = \hat{a}E_0 f(t - (\vec{r} \cdot \hat{k}_i/c))$, is incident on a conducting strip of width w and length L. The strip resides at the dielectric

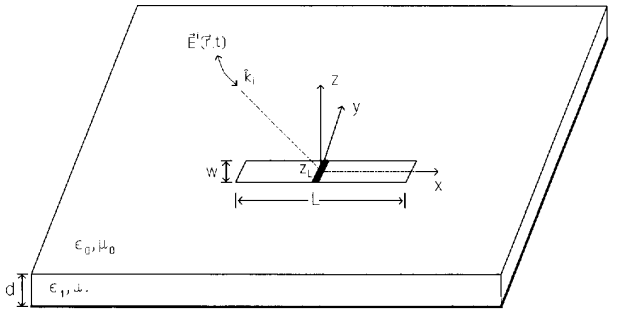

Fig. 1. Geometry of microstrip element.

interface of a grounded dielectric slab of thickness d, having relative permittivity ϵ_r and loss tangent $\tan\delta$.

The electric field in the space above the strip maintained by currents on the strip is

$$\vec{E}(\vec{r}) = \frac{-j\eta_0}{k_0}\int_S \vec{\vec{G}}^e(\vec{r}\mid\vec{r}')\cdot\vec{K}(\vec{r}')\,dS', \tag{1}$$

where $\vec{\vec{G}}^e(\vec{r}\mid\vec{r}')$ is an appropriate electric dyadic Green's function for the layered geometry [7] with the free-space wavenumber and intrinsic impedance given by k_0, η_0, respectively. The Green's function in (1) rigorously accounts for all wave phenomena associated with the conducting element, such as surface-wave excitation and dielectric loss. The current induced on the conductor by some impressed excitation can be obtained by forming an electric field integral equation (EFIE), which enforces the boundary condition for the tangential electric field on the element's surface.

The SEM representation of the current density on the conducting element consists of a series of pole-singularities

$$\vec{K}(\vec{r},\omega) \approx \sum_{q=1}^{2Q}\frac{A_q(\omega_q)\vec{k}_q(\vec{r})}{(\omega-\omega_q)}, \tag{2}$$

where the ω_q's are the complex natural frequencies of the element, distributed symmetrically about the $\mathrm{Im}\{\omega\}$ axis in the upper-half Fourier transform plane. The natural-mode current distribution associated with the q-th natural mode is $\vec{k}_q$, and A_q is the corresponding coupling coefficient [4], [6]. The complex natural resonant frequencies and natural modes are determined by a numerical root search of a homogeneous EFIE [4].

Upon defining a Fourier transform pair

$$\vec{F}(\vec{r},\omega) = \int_{-\infty}^{\infty}\vec{F}(\vec{r},t)e^{-j\omega t}\,dt,$$

$$\vec{F}(\vec{r},t) = \frac{1}{2\pi}\int_{-\infty}^{\infty}\vec{F}(\vec{r},\omega)e^{j\omega t}\,d\omega, \tag{3}$$

the time-domain current can be obtained by standard complex-plane analysis. Ignoring possible branch point singularities, and assuming all pole singularities lie in the upper-half frequency plane, the real line Fourier inversion integral is closed with a semicircle of infinite radius in the lower half plane for $t<0$ to provide a null response. For $t>0$, the inversion integral is closed with a semicircle of infinite radius in the upper-half plane, leading to

$$\vec{K}(\vec{r},t) = -\frac{1}{2\pi}\sum_{q=1}^{2Q}\int_{R_q}\vec{K}(\vec{r},\omega)e^{j\omega t}\,d\omega, \tag{4}$$

where R_q is a small circle surrounding the q-th pole. Upon invoking the SEM expansion (2) for $\vec{K}(\vec{r},\omega)$, and performing the integration around R_q, the time-domain response is found as

$$\vec{K}(\vec{r},t) = \sum_{q=1}^{2Q} jA_q(\omega_q)\vec{k}_q(\vec{r})e^{j\omega_q t}. \tag{5}$$

Exploiting symmetry of the poles, the time-domain current becomes

$$\vec{K}(\vec{r},t) = 2\sum_{q=1}^{Q} e^{-\omega_{qi}t}\,\mathrm{Re}\left\{jA_q(\omega_q)k_q(\vec{r})e^{j\omega_{qr}t}\right\}, \tag{6}$$

where ω_{qi}, ω_{qr} are the imaginary and real parts, respectively, of the q-th complex resonant frequency. The time-domain current density is therefore obtained in closed form subsequent to determination of the object's natural modes.

III. Numerical Results

Numerical results generated with the SEM are presented in the following, and in some cases compared to a numerical inverse Fourier transform (IFT) of a full-wave method of moments (MoM) solution, which is described in [6]. The temporal Fourier inversion of the MoM solution was verified by comparison to results published for a wire above a ground plane without any dielectric present [8]. This comparison was accomplished by setting $\epsilon_r = 1.0$ in the grounded dielectric slab Green's function. The MoM code with numerical inverse Fourier transform inversion was found to be in excellent agreement with the previously published results, and it will be used to verify the SEM solution.

The response of a microstrip element to step and Gaussian excitations will be analyzed here. The step waveform has $f(t) = u(t)$, where $u(t)$ is the unit step waveform. The Gaussian waveform is given by $f(t) = e^{-a^2(t-t_0)^2}$, where $a = 1.665/\sigma$ and $t_0 = 2.1459/a$, with t_0 locating the center of the pulse and σ being the half-amplitude pulse-width [9]. In the following figures, the strip is loaded with a 50 Ω lumped load impedance located at its center, which is the location of the time reference, and all results are presented for E_θ-polarization with $\phi = 0°$. The substrate has $\tan\delta = 0.001$, which is assumed to be constant over the range of frequencies considered here. In Figs. 2 and 3, eight SEM modes were used, whereas in Figs. 4–6 five SEM modes were used.

Fig. 2 shows the voltage induced over the load impedance for an impressed field having a step behavior in time. The voltage is shown as a function of normalized time, where c = speed of light. The element is printed on a dielectric slab ($\epsilon_r = 2.2$) with $d/L = 0.04$ and 0.25 for Figs. 2(a) and (b), respectively. The IFT

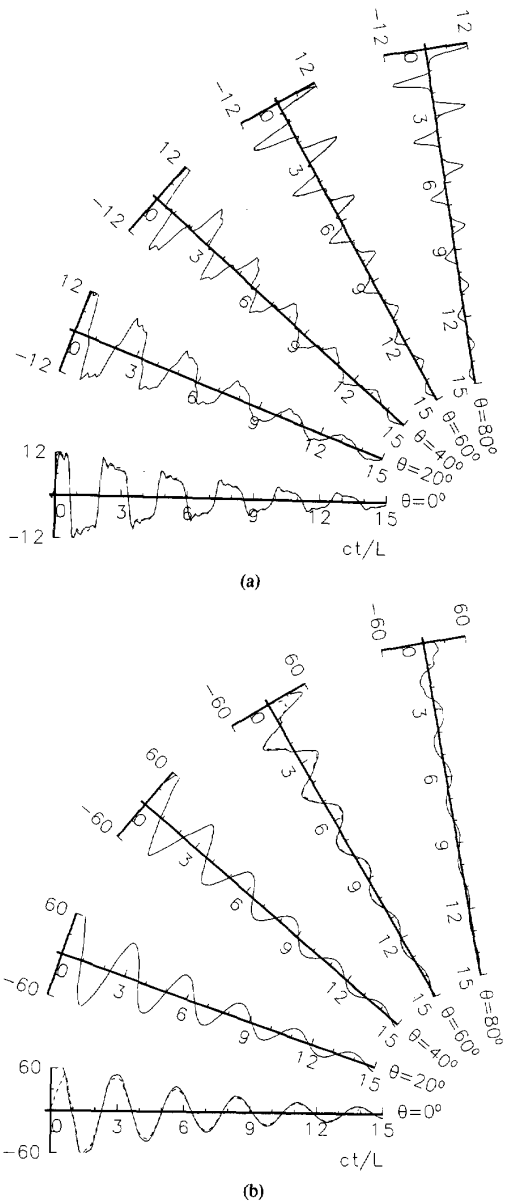

Fig. 2. Induced voltage (mv/E_0L) in a 50 Ω load due to a plane wave step excitation versus normalized time for several incidence angles, (a) $d/L = 0.04$, (b) $d/L = 0.25$. Full-wave MoM solution is also shown (dashed line) for $\theta = 0°$, 60°. $\epsilon_r = 2.2$, $\tan\delta = 0.001$, $W/L = 0.001$.

MoM solution is also shown (dashed line) for $\theta = 0°$ and $\theta = 60°$. For the thin substrate case, the level of the induced voltage is relatively insensitive to the angle of incidence, while the shape of the waveform is highly dependent upon angle. For the thick substrate case the level of the induced voltage is sensitive to the angle of incidence (and is generally larger than for thin substrates), while the shape of the waveform is essentially that of the fundamental mode.

Fig. 3 shows the voltage induced by a step and Gaussian waveform at $\theta = 60°$ for an element printed on a relativity thick substrate, $d/L = 0.25$ with $\epsilon_r = 2.2$. The solid vertical line at

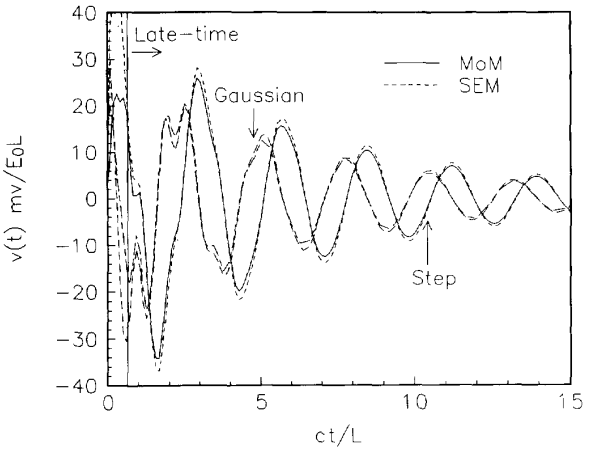

Fig. 3. Induced voltage in a 50 Ω load due to a plane wave excitation versus normalized time for step excitation and Gaussian ($\sigma = .02$) excitations. $\epsilon_r = 2.2$, $\tan\delta = 0.001$, $d/L = 0.25$, $W/L = 0.001$, $\theta = 60°$.

$ct/L \approx 0.75$ shown in Fig. 3 represents the transition between "late-time," where the incident waveform has completely swept past the object and natural resonances have been established, and "early-time," where the incident waveform is illuminating the object. It is well known that the SEM representation (using the form of coupling coefficients shown here, referred to as class-1 coefficients) is most applicable in the late time. For the microstrip geometry, the SEM response does not yield accurate results until the incident waveform has reached the element subsequent to reflection from the ground plane. This delay is so slight for the substrate of thickness $d/L = 0.04$ that it can be ignored.

Fig. 4 shows the SEM-predicted maximum load voltage induced by a step and Gaussian function plane wave, as the substrate thickness is increased. It can be seen that value of the induced voltage increases considerably as the substrate thickness increases. The increase in the magnitude of the induced voltage, as well as the shape of the induced voltage waveforms, can be understood by considering the trajectories of the natural resonances (of an impedance-loaded dipole) in the complex frequency plane, shown in Fig. 5 as substrate thickness and permittivity vary. The first five resonances are shown as substrate thickness varies from $d/L = 0.04$ to 0.475. As the substrate thickness is increased, the fundamental (first) resonance is relativity unaffected, since this mode has a current maximum at the location of the load impedance. The load impedance overwhelms any damping due to radiation or substrate loss, which varies as the substrate thickness changes. The higher order resonances are less affected by the load impedance, and show considerable sensitivity to substrate thickness. For thin substrates the shape of the voltage waveform depends on several natural modes, resulting in the variation of waveform shape with angle shown in Fig. 2(a). For larger values of substrate thickness, the element's response will be increasingly dependent on the fundamental resonance, as the higher-order singularities move away from the $\mathrm{Re}\{\omega\}$ axis. The shape of the induced waveform is seen to rapidly evolve into the temporal oscillation of the fundamental resonance (Fig. 2(b)), which is also expected considering its pole location relative to the higher-order resonances. The radiation resistance for the fundamental resonance of a microstrip dipole radiator generally increases with increasing

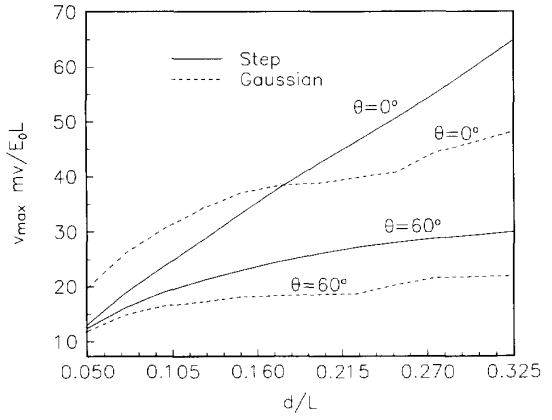

Fig. 4. Maximum induced voltage over a 50 Ω load as a function of substrate thickness. $\epsilon_r = 2.2$, $\tan\delta = 0.001$, $W/L = 0.001$, $\theta = 60°$.

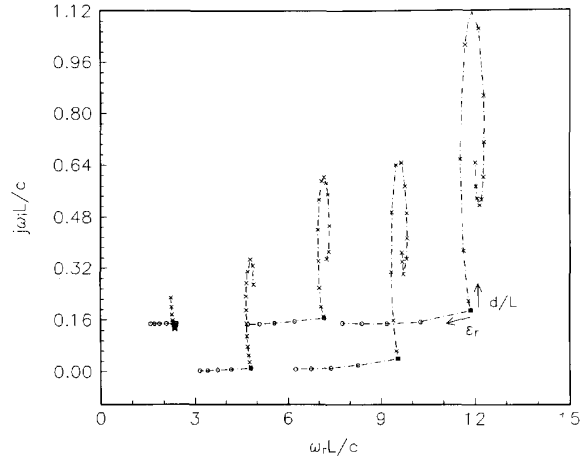

Fig. 5. Trajectories of first-order pole singularities as substrate thickness and permittivity varies. Substrate thickness: $d/L = 0.04$–0.425, substrate permittivity: $\epsilon_r = 2.2$–6.2, $\tan\delta = 0.001$, $W/L = 0.001$.

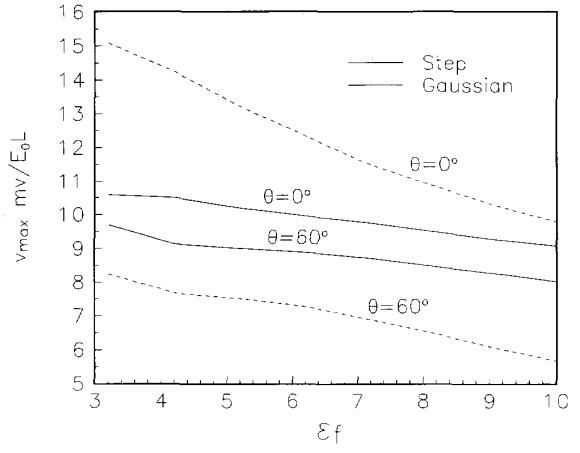

Fig. 6. Maximum induced voltage over a 50 Ω load as a function of substrate permittivity. $\tan\delta = 0.001$, $d/L = 0.04$, $W/L = 0.001$, $\theta = 60°$.

substrate thickness until the onset of the TE_1 surface wave mode [10], which accounts for the increase in the level of the induced waveforms shown in Fig. 4. The level of induced signal depends on angle through the angular dependence of the coupling between the excitation and the fundamental mode.

Fig. 6 shows the variation of the level of the maximum voltage induced by a incident step and Gaussian plane wave, as substrate permittivity is varied for a fixed substrate thickness, $d/L = 0.04$. The loss tangent for all values of permittivity remains at $\tan\delta = 0.001$. It is seen that the maximum level of induced voltage decreases with increasing substrate permittivity, although the variation is relativity less than when the substrate thickness varies. This reduced sensitivity is anticipated by considering the trajectories of the natural resonances as substrate permittivity varies, also shown in Fig. 5. It is seen that the natural resonances tend to move laterally towards lower frequencies as permittivity increases, but remain at approximately the same distance from the real axis.

IV. Conclusion

The singularity expansion method (SEM) has been applied to study the interaction between a transient plane wave and a printed strip antenna. Subsequent to identification of an object's natural frequencies and modes, the SEM formulation results in a closed-form expression for the transient current induced on a microstrip element. By separation of the object's response into excitation independent terms and coupling terms, the time-domain SEM response can be evaluated rapidly for any source orientation or temporal dependence. For the step and Gaussian waveforms considered here, it is found that the level of induced signal increases with increasing substrate thickness over a range of values typically found in microstrip antenna applications. The variation in maximum induced voltage as substrate permittivity is changed is somewhat less than when substrate thickness is varied, although it is found that induced signal levels decrease with increasing permittivity. The shape of the induced voltage or current waveform is highly dependent on the geometric and temporal properties of the source for elements printed on relatively thin substrates. For elements printed on thicker substrates, the shape of the induced waveform is much less sensitive to the form of the excitation, and resembles the oscillation of the object's fundamental resonance.

References

[1] R. Cicchetti, "Transient analysis of radiated field from electric dipoles and microstrip lines," *IEEE Trans. Antennas Propagation*, vol. 39, pp. 910–918, July 1991.

[2] P. Bernardi, R. Cicchetti, and C. Pirone, "Transient response of a microstrip line circuit excited by an external electromagnetic source," *IEEE Trans. Electromagnet. Compat.*, vol. 34, pp. 100–108, May, 1992.

[3] J. Seaux, A. Reineix, B. Jecko, and J. Hamelin, "Transient analysis of space-born microstrip patch antenna illuminated by an electromagnetic pulse," *IEEE Trans. Electromagnet. Compat.*, vol. 33, pp. 224–233, Aug. 1991.

[4] C. E. Baum, "The singularity expansion method," in *Transient Electromagnetic Fields*, L. B. Felson, ed. New York: Springer-Verlag, 1976, pp. 128–177.

[5] C. E. Baum, "The singularity expansion method: Background and developments," *IEEE Antennas Propagation Soc. Newsletter*, pp. 15–23, Aug. 1986.

[6] G. W. Hanson and D. P. Nyquist, "The RCS of a microstrip dipole deduced from an expansion of pole-singularities," *IEEE Trans. Antennas Propagation*, vol. 41, pp. 376–379, Mar. 1993.

[7] J. S. Bagby and D. P. Nyquist, "Dyadic Green's functions for integrated electronic and optical circuits," *IEEE Trans. Microwave Theory Technol.*, vol. MTT-35, pp. 206–210, Feb. 1987.

[8] K. Umashankar, T. H. Shumpert, and D. R. Wilton, "Scattering by a thin wire parallel to a ground plane using the singularity expansion method," *IEEE Trans. Antennas Propagation*, vol. 23, pp. 178–184, Mar. 1975.

[9] J. Herault, R. Moini, A. Reineix, and B. Jecko, "A new approach to microstrip antennas using a mixed analysis: transient frequency," *IEEE Trans. Antennas Propagation*, vol. 38, pp. 1166–1175, Aug. 1990.

[10] P. B. Katehi and N. G. Alexopoulos, "On the effect of substrate thickness and permittivity on printed circuit dipole properties," *IEEE Trans. Antennas Propagation*, vol. 31, pp. 34–39, Jan. 1983.